

Manganese nodule morphology as indicators for oceanic processes in the Central Indian Basin

T.C. Vineesh^{*}, B. Nagender Nath, R. Banerjee, S. Jaisankar and V. Lekshmi

Abstract

In order to understand the role of geological features in the depositional environment and the prevailing oceanic processes on the formation and characteristics of manganese nodules, a detailed morphological study of the manganese nodules was undertaken on 23,000 nodules from 194 locations (including 801 sub-stations) in a nodule rich area covering about 150,000 sq. km in the Central Indian Basin (CIB). Nodules with rough surface texture dominate most of the area except the south-eastern part of the basin, which is floored more by the smooth nodules. Smaller nodules (< 4 cm) are common and are dominant both in density and mass in the south-eastern part of the basin, whereas north-western part and the central part show dominance of larger rough nodules with higher density and mass. Smooth nodules are also found in shallower depth (< 5000m), on the seamount tops and along the slopes, whereas the rough nodules are mostly seen in deeper areas. Significantly, eastern part of the basin show smooth nodules with smaller size. Smooth nodules > 4cm diameter are rare and show low oxide layer thickness and low bio-sediment remnants compared

^{*}T.C. vineesh (✉), B. Nagender Nath, R Banerjee, S Jaisankar, V.Lakshmi

Geological Oceanography Division, National Institute of Oceanography, (Council of Scientific and Industrial Research)

Dona Paula, Goa.40304 India. Email: cvineesh@nio.org, Tel: +91 8322450498, Fax: +91 8322450609

to rough surfaced nodules. Large variation in morphological types of nodules are found in CIB with spheroidal, oblong, triangular, rounded, sub-rounded or irregular shapes, with irregular nodules being most common. Most common nucleus is altered basalt, while pumice, shark teeth, clay and older nodule nuclei are also seen. Water currents and seafloor topography seem to play a major role in defining the nodule morphology. The results of the study show the abundance of smaller nodules with smooth surface texture towards the eastern side of the study area. These features are probably responding to the bottom current activity. It is suggested here that since the eastern part of the study area is closer to the saddles in the 90°E ridge (which is the entry point of the Antarctic Bottom Water (AABW) currents into the CIB), the influence of AABW is reflected in the shape and size of the nodule in this area.

Key words: Polymetallic nodules, morphology, Central Indian Basin, Antarctic Bottom water.

Introduction

Polymetallic nodules cover an area of approximately 54×10^6 km² in the world oceans. The most extensive nodule fields are found in the Pacific Ocean. The nodules are spread about 23×10^6 km² in the Pacific Ocean. The Atlantic Ocean has the lowest distribution, with an area of about 8×10^6 km². Indian Ocean has a nodule field spread over $10-15 \times 10^6$ km².

In the Indian Ocean, the nodules are distributed in the Crozet basin, the Wharton basin, the Somali basin and the CIB, and richest among them are found in the CIB. Ridge system on the three sides of CIB (Kamesh Raju, 1993) inhibits the supply of lithogenic input and provides a favorable environment for the formation and

growth of the polymetallic nodules. It receives sediments mainly from north (Ganges and Bhramaputra) (Nath et al., 1989; Nath, 2001) resulting in low nodule abundance in the northern CIB. CIB is also protected from circum polar bottom currents and Antarctic Bottom Water currents by these three major ridge systems, but the AABW enters through the deep saddles on the Ninety East Ridge (5°S and 10°S) in to the CIB and spreads northward(Jauhari and Pattan, 2000 and the references therein). Gordon et al.,(2002) clearly demonstrated the entry of AABW currents into the CIB from nutrient rich benthic layers and argued for its influence extending up to Bay of Bengal. Would this have any influence on the characteristics and formation of CIB nodule is not known.

The nodules in the CIB vary in size, shape and surface texture. Earlier studies have shown that the environment of deposition of polymetallic nodules is characterized by several parameters such as sea floor morphology, sediment types, water depth and water column conditions, surface productivity and distance from shore (Banerjee and Miura, 2001; Jauhari, 1987; Sudhakar, 1989; Ghosh and Mukhopadhyay, 1999). The formation of the ferromanganese deposits of CIB appears to have begun during Late Miocene–Early Pliocene (~8–3 Ma) (Ghosh and Mukhopadhyay, 1999). The CIB nodules are mostly first generation nodules (Ghosh and Mukhopadhyay, 1999).

The objective of this study is to map the morphological variations of the CIB polymetallic nodules spatially and decipher the controls of basin morphology and prevailing oceanographic processes on these variations. Also determined are the oxide layer thickness and their relation to the surface texture. To our knowledge, this

represents the largest and systematic study on CIB nodule morphology undertaken so far.

Materials and Methods

We have examined around 23,000 nodules from 194 stations (including 801 substations) in a nodule rich area of 1,275,000 sq. km in the CIB. This area lies between 7°S to 16°30'S and 72° E to 83°30' E (Fig. 1) and the stations were selected at a grid of ½ degree spacing. The nodules have been collected mainly by free fall, VanVeen and Peterson grabs by the National Institute of Oceanography, India, as a part of their polymetallic nodule exploration programme. The nodules were classified into various classes at two-centimetre size intervals. The variation in size and weight of nodule population among all stations with respect to latitude and longitude were studied. The shape, nucleus types and surface texture of each of the nodule studied and the general dominating shapes and surface texture of each size class are noted and are plotted on the map to study its variation and distribution throughout in the entire basin. For the oxide layer thickness study, we took one representative nodule from each substation and measured the average thickness of oxide layer using vernier-callipers.

Geological setting

The Central Indian Basin is bounded by ridge systems except in the northern side. Central Indian ridge acts as a barrier to the entering of strong bottom water currents to CIB from Madagascar basin and Crozet basin. The sedimentation rate in CIB is very low (2.7 mm/ka 14°S and 78°E, 3.4 mm/ka 10°S and 82°E) (Udintsev, 1975; Banakar et al., 1996; Borole, 1993) . General topography of the basin varies

with small abyssal hills to seamounts giving rough bottom morphology. Around 200 seamounts are reported from CIB (Das et al., 2007 and references therein). The CIB can be divided into two distinct regions, the highly deformed north (above 9°S) and northeastern part and the relatively undeformed southern part (below 9°S). The central part of the CIB is characterized by siliceous radiolarian ooze and the southern part by red clay (Udintsev, 1975; Nath et al., 1989; Nath, 2001). The basement age of CIB is reported to be 50-60 Ma (Mukhopadhyay et al., 1995) and is covered with terrigenous sediments on the northern part (up to 5°S latitude), from 5°S to 14.5°S the major sediment type is siliceous oozes with sporadic calcareous patches found at around 12-14°S latitude and 82.5-83.5°E longitudes. The southern part of the basin (south of latitude 14.5°S) is covered with red clay (Nath et al., 1989). Three major fracture zones along 73°E (Vishnu Fracture Zone), 76.5°E (triple junction trace on the Indian plate-TJT-In) and 79°E (Indrani) are identified trending almost north south in this basin (Kamesh Raju, 1993). Majority of the CIB seamounts were formed during the period 61 to 52 Ma, and the formation of seamounts peaked between 56 to 52 Ma (Das et al., 2007). This closely corresponds with the Indo-Eurasian collision event, during which time the spreading rate increased (95–55 mm/yr) (Das et al., 2007).

Results

Size:

The size of CIB nodules ranges from less than 1 cm to more than 10 cm in diameter and smaller nodules <4 cm are common in CIB (Valsangkar and Khadge, 1989). In this present study, we classified all the nodules into five classes with two-centimetre intervals like 0-2, 2-4, 4-6, 6-8, and above 8 cm. Smaller nodules (< 4cm)

dominate the entire basin with nodules of 0-2cm size class dominating the eastern part of the basin, northern side of the study area and small patches on the seamount tops. Other class of smaller nodules (2-4 cm size range) is the dominant size class in CIB, in eastern and southern part of the study area except deep basins (Fig. 2). Larger nodules (>4 cm) dominate in the areas of deep basins. Among these 4-6 cm sized nodules are abundant in the northwestern part of the CIB, while those between 6 and 8 cm are limited to central deep basins only (Fig. 3).

Nodule nucleus

The distribution and morphology of the nodules are controlled by the availability of nucleus materials on which metallic oxides can accrete (Glasby, 1973; Glasby and Read, 1976; Horn et al., 1973). The shape of the nodules usually follows the shape of the nucleus. Topographic highs are dominated by encrustations. Topographic slopes, flanks and abyssal plains are dominated by exposed nodules cover. Fresh basalts occur at the summits of the abyssal hills and weathered basalts and pumice occur on the slopes and the abyssal plains. In the study area, we observed different types of nodule nucleus and most common nucleus is altered basalt (Fig. 4). Nearly 90% of the stations show altered basalt as nucleus (Fig. 5). While in some locations, though altered basalt is the dominant nucleus type minor contributions of pumice were found as nodule nucleus, but only in some locations are dominated by pumice nucleus. Shark teeth and hardened clay also found rarely (Fig. 4). Pumice nucleus types are mainly distributed in both sides of 76.5° and 79° E fracture zone between 10.5° and 14.5°S. While Pattan et al.(2008) have attributed the occurrence of CIB pumice to distal source of Indonesian volcanic arc, Iyer and Sudhakar (1993) have attributed the presence of pumice along the fracture zone to intraplate volcanism.

Occurrences of nodules with shark teeth as nucleus types are concentrated in central southern and south eastern part of the study area (Fig. 5).

Shape

Irrespective of the size class they belong to, irregular nodules predominate in the entire CIB (Fig. 6). Smaller nodules are comparatively more rounded, subrounded or spheroidal. Larger nodules have shown irregular, elongated, tabular, triangular and mammillated shapes. The shapes of most nodules were found to be closely related to the substrate or nucleus in which they grew. Irregular shaped nodules were generally found to have altered basalt as nucleus. The topography of the area seems to be the major controlling factor on the shape of nodule in CIB. Different shaped nodules are present within the same station suggesting a local variability (Mukhopadhyay and Nath, 1988). According to the degree of roundness, we classified the stations into fourteen classes (Fig. 6 a-d). Spheroidal and sub-rounded smaller nodules (<4cm) are predominant in the deep basins of the western, central eastern and south-eastern parts of the study area. Irregular, flat and discoidal smaller nodules are mainly associated with topographic highs and seamounts of rugged topography. Irregular nodules of the same size class are most common on seamounts (Fig 6). In general, the degree of roundness of small nodules (<4cm) increase from topographic high towards the deep basins.

Irregular nodules are most common in large nodule size classes (>4cm). Sub-rounded, spheroidal, oval shaped nodules of 4-6cm size class are again limited to the deep basinal area between the seamount chains related to 76.5 and 79 °E fracture zones and eastern part of the area (Fig 8). Sub-rounded nodules in higher size classes

(6-8cm and >8cm) are rarely found and are distributed in deep basins. The areas related to seamounts are showing irregular nodules where altered basalt is the dominant nucleus which may be controlling the shape of CIB nodules. Deep basins in between the seamounts chains with pumice as the major nucleus type shows increasing degree of roundness. Triangular nodules are concentrated in areas where the shark teeth as nucleus dominant. From all these we conclude that the shape of nodules directly depend on size, shape and availability of nucleating materials and topography of the area.

Thickness of oxide layer

The thickness of the oxide layer over the nucleus is the clear indication of the age of nodules and mode of accretion. From the internal layering we can identify the environment of deposition. Thicker oxide layers either suggest that they are more aged or metal oxides have accreted faster. In this study, we found that the stronger the substrate, more the oxide thickness. The oxide layer over altered basalt, older nodule nucleus and shark teeth show thicker oxide layer deposition than over the pumice. The nodules with both clayey nucleus and fresh basalt as nucleus show very less oxide thickness, which may be due to the younger age. Biogenic remnants are also less in smooth nodules. Sediment types also play some role in the thickness of the oxide layer. Oxide layer thickness is thinner in the nodules from the terrigenous, terrigenous-siliceous and red clay sediments. More thick oxide layers are reported from the areas of siliceous, calcareous and siliceous-red clay sediments (Banerjee and Miura, 2001). A total of 106 smooth nodules and 216 rough nodules were observed and the thickness varied between 0.1 to 7 mm. Rough nodules were found to have slightly high oxide layer thickness (average 2.7 mm) than the smooth nodules

(average 2.6 mm). In some of the mixed nodules, we found that one side is thicker than the other side of the same nodule. It is prominent in some mixed type of nodules suggesting different accretion rates on two sides. Mostly the upper side of the nodule facing water column is smoother and has very less biogenic remnants on their surfaces, compared to the lower side in which is buried in sediments showing more thickness and high biogenic remnants and sediment remains. Most of the rough nodules show high biologic traces on their surfaces and are more prominent in the nodules at water sediment interface. Thus the rough nodules are apparently suitable habitat for organisms. The bottom rough side of some nodules show little brownish colour may be due to the sediment influence supports the distinct top-bottom elemental fractionation noticed before (Nath, et al., 1992).

Surface texture

The dominant surface texture of the CIB nodules was found to be rough. Eastern part of the area between 10-13°S shows smooth and mixed surface texture (figure 7). The central part of the basin (74.5° E to 78°E) shows abundant rough textured nodules which may be due to the presence of more number of seamounts with a rugged topography (Mukhopadhyay, et al.,1995; Kodagali, 1995). Spheroidal and ellipsoidal nodules with rough surface are more common among smaller nodules in CIB (Jauhari, and Pattan, 2000). Size, in contrast, does show some relationship to surface texture. Generally, smooth texture is associated with smaller nodules and rough texture with larger nodules. Nodules with smooth texture are generally smaller than 4 cm which is consistent with previous studies (Banerjee and Miura, 2001). Earlier workers proposed nodules with rough surface textures are associated with siliceous radiolarian sediments, whereas smooth-surface nodules are more common in

the pelagic clay domain (Banerjee and Miura, 2001; Jauhari, 1990; Rao, 1987) arguing for siliceous sediments to favour rough surface texture and the pelagic red clay bearing smooth textured nodules. However, our study shows that the smooth surfaced nodules can also occur in the siliceous oozes (Fig. 8). Smooth and mixed surface texture is dominant in areas of seamount slope and foot hills or relatively shallower water depth. Smooth nodules in the eastern area seem to be mainly due to strong current system prevailed in this area. Some locations or small patches of smooth surface texture in the north western part of study area are due to the presence of rugged topography and local current system.

Nodules in the eastern part of the study area are probably affected by the strong bottom currents from Ninety East ridge (Antarctic bottom water currents from 5° and 10°S saddles of the Ninety East Ridge system). Bottom current velocity may play more important role in influencing the nodule morphology. Large spheroidal nodules may form in areas of strong bottom currents, where sediment accumulation may be minimal. The smaller spheroidal nodules with uniform surface texture on all sides show the influence of rolling due to the bottom currents, and they are more mobile on the sea floor as compared to the larger nodules (Glasby, 1977). The rolling and the effect of forces acting on the sediment-water interface influence the surface textures of the nodules (Glasby, 1977). The smaller nodules are more mobile on the sea floor and hence their surfaces may have become smooth.

The surface texture of the nodule is closely related to the topography and water depth. In this study, we observed that all the stations (except two) with smooth surface texture are found at water depths shallower than 5200 m, and very rough surface nodules in deeper areas suggesting a clear topographic control.

General chemistry of CIB nodules:

We selected analytical data of nodules from 54 different locations (Banerjee and Miura, 2001; Jauhari, 1990), with one degree intervals for a comparative study of latitudinal and longitudinal control on geochemical variation of nodules. The Mn/Fe ratio in the CIB nodules vary from 0.96 to 8.76 but most of them fall within the field of hydrogenous (Mn/Fe ratio <2.5) deposits (Jauhari, 1987 and references therein). Mn/Fe ratio is the direct indicator for the genesis of the manganese nodules and different depositional processes. The variations in the Mn/Fe ratio reflect variability in the composition of bottom water. Earlier workers reported the higher concentrations of Mn, Ni and Cu in the nodules from siliceous sediments, reflecting the influence of early diagenesis of the biogenic components, whereas the higher Fe and Co contents in the nodules occurring in red clay areas are a result of their precipitation as authigenic oxyhydroxides (Rao, 1987; Jauhari, 1989; Sudhakar, 1989). Along 11° S latitude, Mn/Fe value varies from 2.7 to 9.44 and except at 73°E and 83°E, where all are above 5 indicating their diagenetic formation. Along 14°S latitude, nodules from western region (74°E to 76°E) and eastern end (82°E) of the basin, show higher Mn concentration and higher Mn/Fe compared to those from eastern region (76°E to 80°E) where Fe content is high (Fig. 9 a-d).

The nodules from central part of the CIB (12 to 14°S and 75 to 79° E) with siliceous sediments as their substratum show high Mn/ Fe values. Whereas, nodules from the northern region show low Mn/Fe where the terrigenous input is more. Southeastern part of the study area also show low Mn/Fe where small iron rich smooth nodules occur suggesting hydrogenetic formation processes. Nodules from deep basins in between seamount chains show high Mn concentration. Fe content is

more in areas of topographic highs and at south eastern part of the CIB. Cobalt content is high only in the southeastern part of the CIB (Figure 9,b and 9,d). From all these, we conclude that the nodules occurring in the central part of the study area (12-14° S and 74-78°E) are diagenetic in nature and are less affected by strong water current systems. Southeastern part of the basin support mostly iron rich smooth nodules and are likely affected by AABW currents from 90°E Ridge saddles.

Discussion and conclusion

Morphology of the nodules in the Central Indian Basin is controlled by topography of the area, bottom water currents, water column depth, sedimentation rate, movement of nodules, metal oxide input rates, the sediment types etc. Among all these, topography of the area, bottom water currents and water depth seem to play more effective role in controlling the nodule facies. Variability of nodule surface morphology was earlier attributed to sedimentary conditions. However, our data shown that the southeastern part of the basin, smaller nodules with smooth or mixed surface texture are more in number, which may be controlled by the seafloor topography and AABW currents entering in to the basin through the saddles in the 90°E Ridge system (Fig. 10). Thus, the bottom water currents seem to may play an important role influencing the manganese nodule morphology, growth rates and chemistry in the CIB. The effects of strong bottom water currents in deep-sea environment are mainly of two types; sediment erosion and rolling movements of surface nodules. Both processes inhibit the nodule growth. Bottom photographs from the Southeast Indian Ocean shows the presence of smaller nodules in the areas of strong bottom water currents indicated by ripple marks and channels (Kennet, 1991). Hiatuses in manganese nodule growth due to the erosional effect of Antarctic bottom

water currents co-incident with global climatic changes were well established (Glasby, 1986). Bottom water currents may induce changes in position of nodules or rolling movement along with eroding sediment (Glasby, 1986). Penrhyn basin experiences strong Antarctic bottom water current activity. The photographs of nodule covering seabed from this area shows dominantly smaller nodules with spheroidal and ellipsoidal shapes (Glasby, 1986).

In the northwest and the central part of the CIB, nodules are found to be more rough or gritty in surface texture. Their shapes also vary and are mainly controlled by the rugged topography and number of seamounts. The effect of AABW current is less in this area. Water column depth also plays an important role in shaping the surface morphology of the nodules. Local nodule formation facies exist in the northwestern part of the basin indicated by small patches of smooth surface texture.

The chemistry of the CIB nodules from the central deep basins, which is located between the seamount chains are probably, related to the major fracture zones. These areas are covered with larger rough nodules, and these are older nodules in this basin. Nodules from seamount top are mainly smaller smooth nodules and are probably younger in age (Pleistocene). In CIB, the formation of nodules seems to have started in the deeper part of the basin in the central region around the late Miocene age. These nodules act as the sink for different metals in CIB from late Miocene time. And also the chemistry data suggests that the older nodules in deeper basins are more influenced by early diagenetic processes in view of the lack of significant influence of AABW. The formation of the nodules was later extended to the other part of the basin in the course of time. During the Pleistocene, major bottom water currents (AABW) affected the nodule formation and growth, leading to the

formation of smaller nodules with smooth surface texture in the eastern part of the basin. The central and northern parts of the study area are protected from these currents due to the presence of major seamount chains.

Acknowledgements

Our sincere thanks to Director, NIO and M. Shyam Prasad for his encouragement and constant support. Ministry of Earth Sciences (formerly DOD), Government of India is thanked for ship time and funding the project Polymetallic Nodules surveys. This is NIO contribution no.4436

REFERENCES

- Banakar, V.K., Gupta, S.M., Padmavati, V.K., 1991, Abyssal sediment erosion from the Central Indian Basin: Evidence from radiochemical and radiolarian studies: *Mar. Geol.*, v. 96, p.167-173.
- Borole, D.V., 1993, Late Pleistocene sedimentation: A case study of the central Indian Ocean Basin: *Deep-Sea Res.*, v. 40(4), p. 761-775.
- Banerjee, R., Miura, H., 2001, Distribution pattern and morphological relationships of manganese nodules from Central Indian Ocean basin; *Geo-Mar. Letts.*, v. 21(1), p. 34-41.
- Das, P., Iyer, S.D., Kodagali, V.N., 2007, Morphological characteristics and emplacement mechanism of the seamounts in the Central Indian Ocean Basin: *Tectonophysics.*, v. 443(1-2), p.1-18.

- Ghosh, A.K. and Mukhopadhyay, R., 1999, Mineral wealth of the Ocean: A treatise on distribution, origin, exploration, mining and management of sea floor non-living resources: Oxford & IBH, New Delhi, India, p. 255.
- Glasby, G.P., 1973, Role of sub-marine volcanism in controlling the genesis of marine manganese nodules: *Oceangr. Mar. Biol. Ann. Rev.*, v. 11, p. 27.
- Glasby, G.P. and Read, A.J., 1976, Deep-sea manganese nodules: *in* Wolf, K.H. Ed., Handbook of Strata-Bound and Stratiform Ore deposits: Elsevier, Amsterdam, p. 295--340.
- Glasby, G.P., 1977, Why manganese nodules remain at the sediment-water interface: *N. A. J. Sci.*, v. 20, p. 187-190.
- Glasby, G. P., 1986, Hiatuses in manganese nodule growth: relation to bottom current activity?: *Geo-Mar. Letts.*, v. 4, p. 247-252.
- Gordon, A.L., Claudia, F., Giulivi, T.T., Stewart, S., John, M. and Donald O., 2002, Bay of Bengal nutrient-rich benthic layer: *Deep-Sea Res. II.*, v. 49, p. 1411–1421.
- Horn, D.R., Horn, B.M., and Delach, M.N., 1973, Factors which control the distribution of ferromanganese nodules and proposed research vessel tracks in the North Pacific: Lamont Doherty Geological Observatory Technical Report v. 8, p. 1-20.

- Iyer, S.D., Sudhakar, M., 1993, Coexistence of pumice and manganese nodule fields- evidence for submarine silicic volcanism in the Central Indian Basin: Deep-Sea Res. v. 40(5), p.1123-1129.
- Jauhari, P., 1987, Classification and inter-element relationships of ferromanganese nodules from the Central Indian Ocean Basin: Mar. Min. v. 6, p. 419-429.
- Jauhari, P., 1989, Variability of Mn, Fe, Ni, Cu and Co in manganese nodules from the Central Indian Ocean Basin: Mar. Geol., v. 86, p. 237-242.
- Jauhari, P., 1990, Relationship between morphology and composition of manganese nodules from the Central Indian Ocean: Mar. Geol., v. 92, p.115-125.
- Jauhari, P., and Pattan, J.N., 2000, Ferromanganese nodules from the Central Indian Ocean Basin, *in* Cronan, D.S, Ed., Handbook of marine mineral deposits: CRC Press, USA, p.171-195.
- Kamesh Raju, K.A., 1993, Magnetic lineations, fracture zones and seamounts in the Central Indian Basin. Mar. Geol., v.109(3-4), p.195-201.
- Kennett, J., 1991, Marine Geology: Prentice Hall, International Inc. London. p. 495-501.
- Kodagali, V.N., 1995. Influence of bathymetry in manganese nodule pilot mine site selection: A case study from the Central Indian Basin, *in* Yamazaki, T., Aso, K., Okano, Y., Tsurusaki, K. Eds.,The Proceedings of the First (1995) ISOPE Ocean Mining Symposium: ISOPE Ocean Mining Symp., Tsukuba, Japan. Int. Soc. of Offshore and Polar-Eng.(ISOPE), Colorado, USA, p. 99-104.

- Mukhopadhyay, R., Batiza, R., Iyer, S.D., 1995, Petrology of seamounts in the Central Indian Ocean Basin: Evidence for near-axis origin: *Geo-Mar. Letts.*, v. 15(2), p. 106-110.
- Mukhopadhyay, R., Nath, B.N., 1988, Influence of seamount topography on the local facies variation in ferromanganese deposits in the Indian Ocean: *Deep-Sea Res.*, v. 35, p. 1431-1436.
- Nath, B.N., 2001, Geochemistry of sediments: *in* SenGupta, R., Desa, E. Eds., *The Indian Ocean: A perspective*: Oxford & IBH; New Delhi (India), v. 2, p. 645-689.
- Nath, B.N., Balaram, V., Sudhakar, M., Pluger, W.L., 1992, Rare earth element geochemistry of ferromanganese deposits of the Indian Ocean: *Mar. Chem.*, v. 38, p. 185-208.
- Nath, B.N., Rao, V.P.C. and Becker K.P., 1989, Geochemical evidence of terrigenous influence in deep-sea sediments up to 8°S in the Central Indian Basin. *Mar. Geo.*, v. 87, p. 301–313.
- Pattan, J.N., Mudholkar, A.V., JaiSankar, S., Ilangovan, D., 2008, Drift pumice in the Central Indian Ocean Basin: Geochemical evidence: *Deep-Sea Res.* v. 55(3), p. 369-378.
- Rao, V.P., 1987, Mineralogy of polymetallic nodules and associated sediments from the Central Indian Ocean Basin: *Mar. Geol.*, v. 74, p. 151-157.
- Sudhakar, M., 1989, Ore grade manganese nodules from the central Indian basin: an evaluation. *Mar. Min.*, v. 8(2), p. 201-214.

Udintsev G.B., 1975, Geological and Geophysical Atlas of the Indian Ocean,
Udintsev G.B, Ed., Academy Science, USSR, Moscow, p.23.

Valsangkar, A.B., Khadge, N.H., 1989, Size analyses and geochemistry of
ferromanganese nodules from the Central Indian Ocean Basin: Mar. Min., v.
8(3), p. 325-347.

Figure Captions:

Figure 1: Map showing sampling locations in the Central Indian Basin. Inset shows the study area with respect to India and topographic feature.

Figure 2: Distribution of small nodules in number percentage (colour coded) with respect to topography (black).

a) 0-2 cm size intervals; b) 2-4 cm size intervals.

Figure 3: Distribution of larger nodules in number percentage (colour coded) with respect to topography (black).

a) 4-6 cm size intervals; b) 6-8 cm size intervals.

Figure 4: Different types of nuclei observed in CIB nodules.

Figure 5: Distribution of different nucleus types observed in CIB nodules. As shown basalt is the most dominant nucleus type.

Figure 6: Variation in shape of the nodules (colour coded) with topography (black).

Shape is classified into 14 types in the order of increasing irregularity in shape.

a) 0-2 cm; b) 2-4 cm; c) 4-6 cm; d) 6-8 cm

Figure 7: General surface texture of nodules from different sampling locations with bathymetry (200 m interval contours). Surface texture is marked with symbols S,R and M abbreviated for smooth, rough and mixed type of nodules.

Figure 8: Sampling locations and nodule surface texture with respect to general sediment type distribution (Sediment distribution map from Nath et. al, 1992)

Figure 9: Chemical variation of CIB nodules (data from Jauhari 1990 and Banerjee et.al 2001)

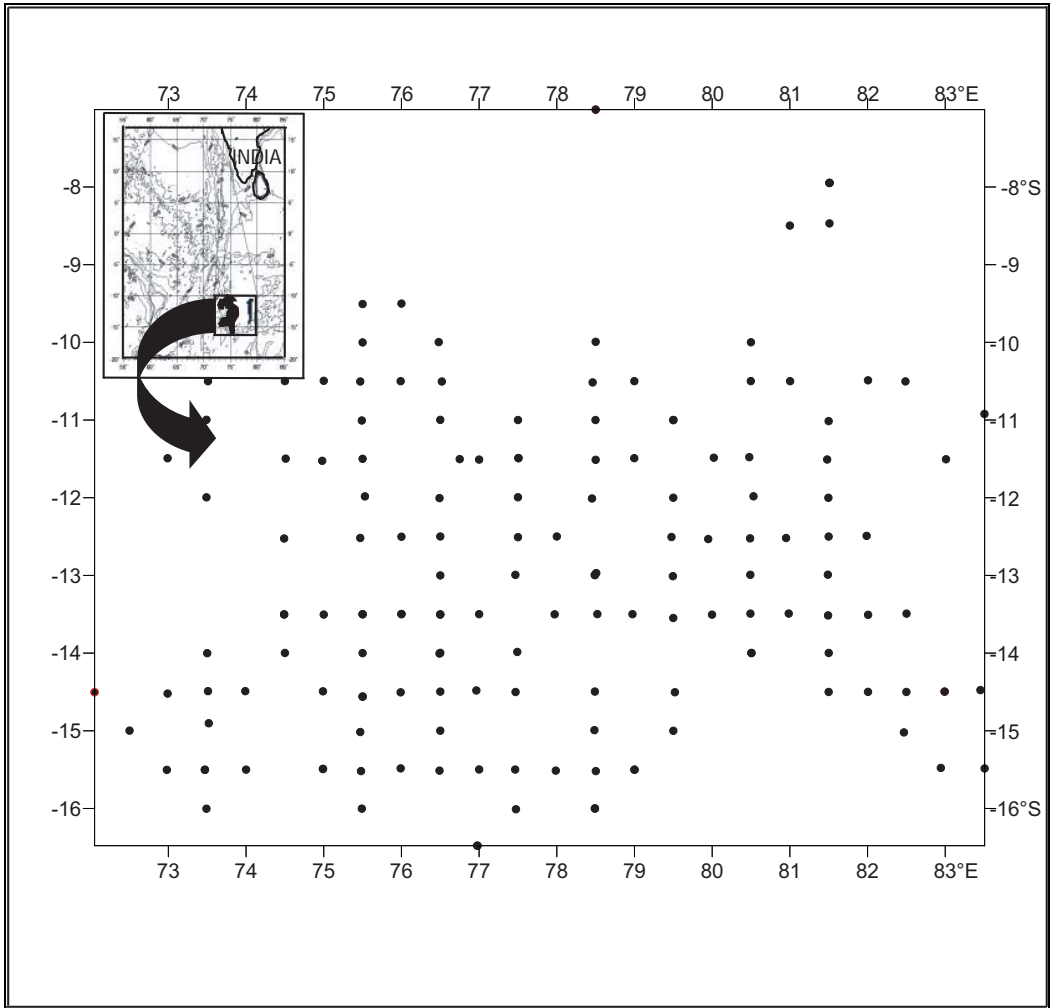
(a) Manganese content (%)

(b) Iron content (%)

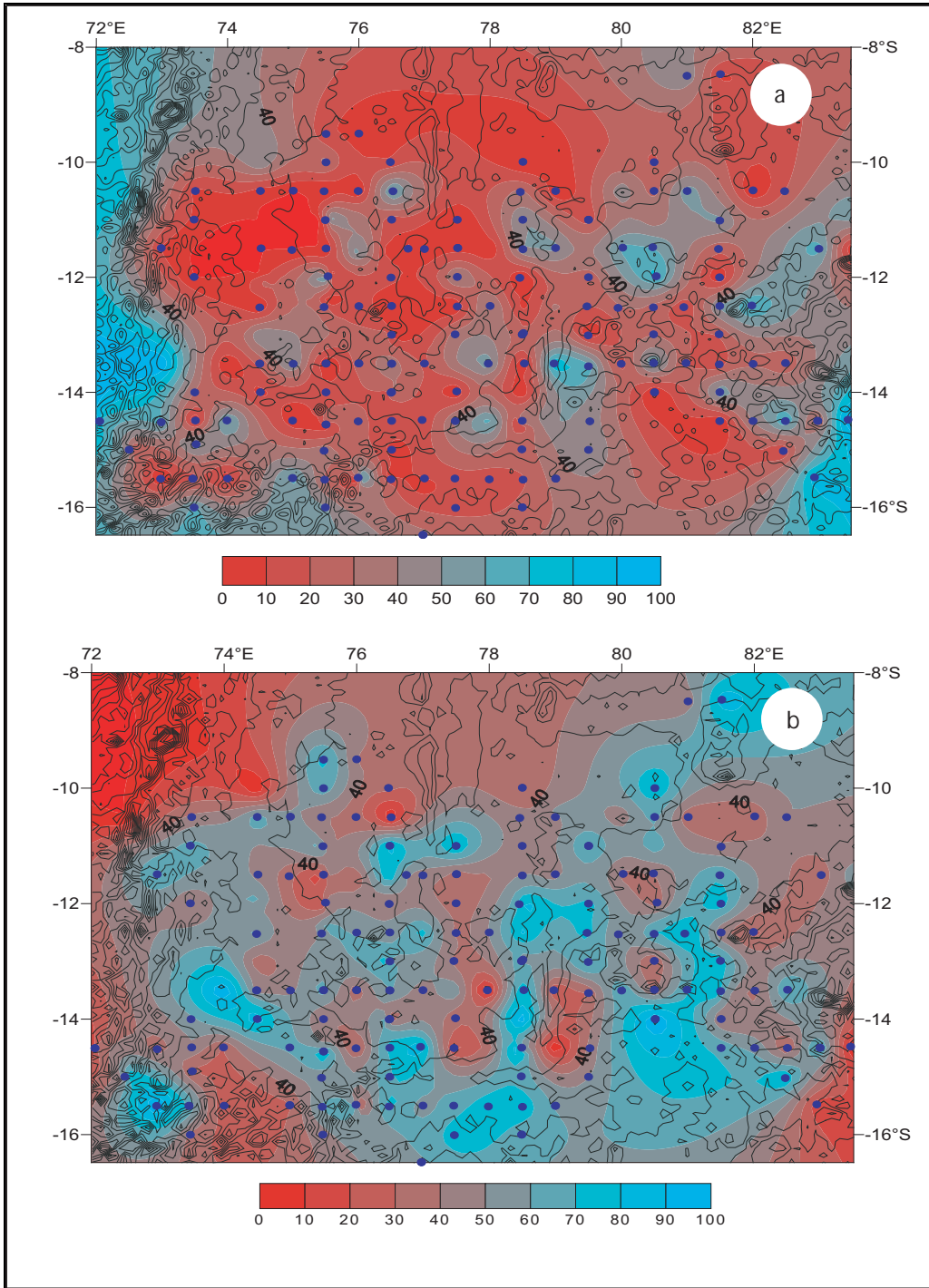
(c) Mn/Fe ratios

(d) Cobalt content (%)

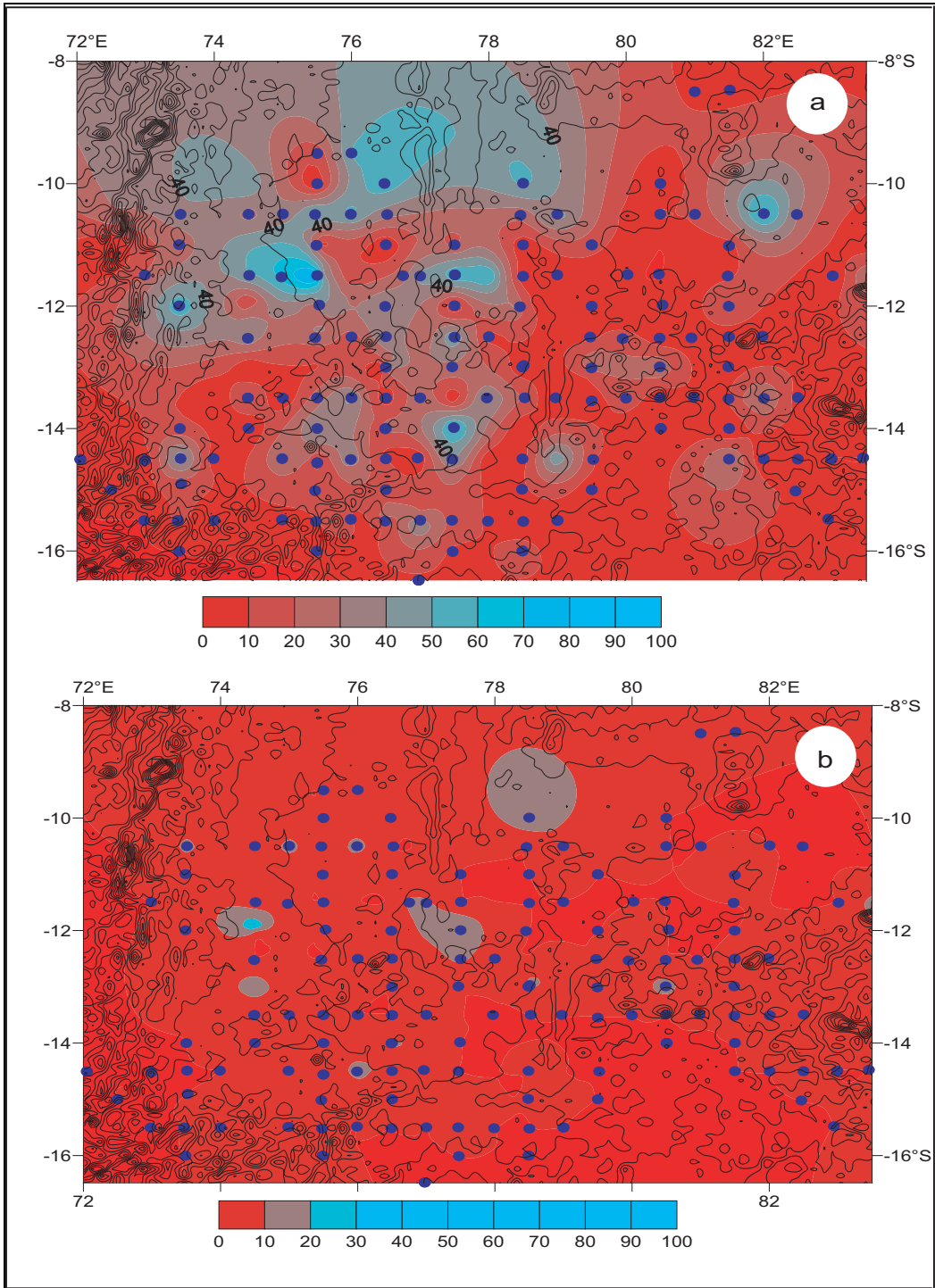
Figure 10: Entrance of AABW currents in to CIB through deep saddles (5 and 10°S) of 90°E Ridge System (adopted from Gordon et.al 2002). Red box shown in the SW corner is the present study area.



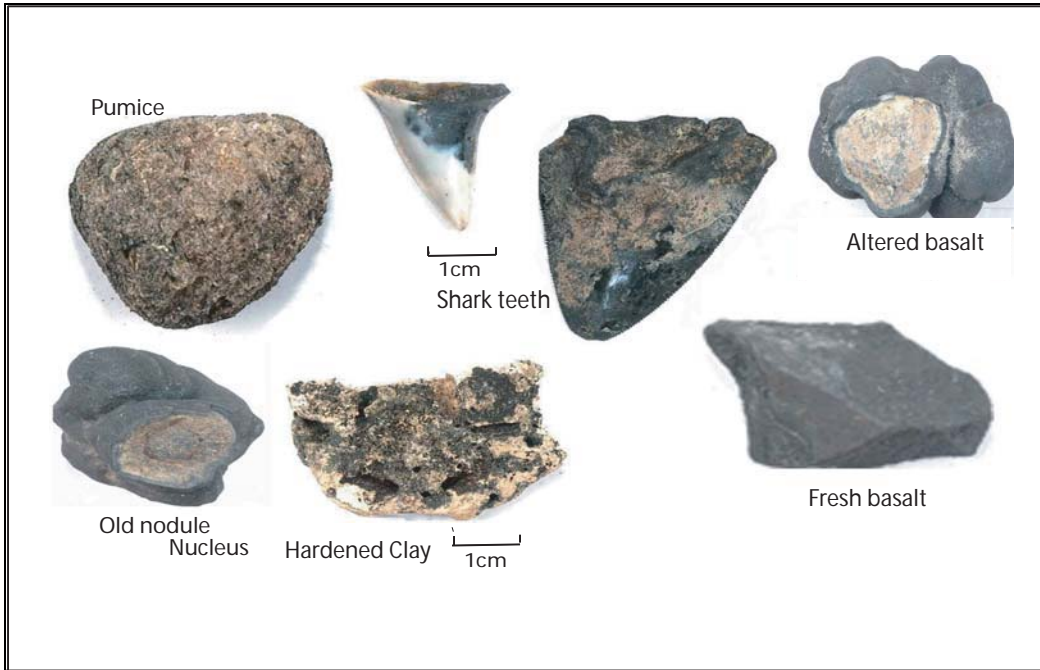
Vineesh et al Figure 1



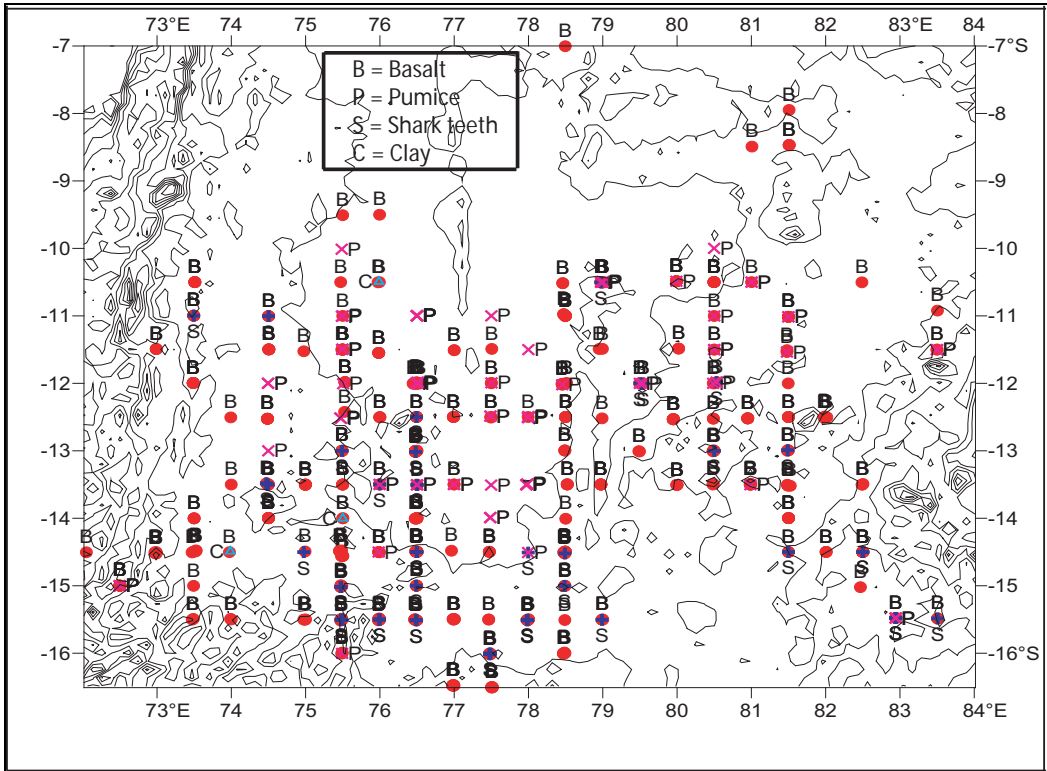
Vineesh et al Figure 2



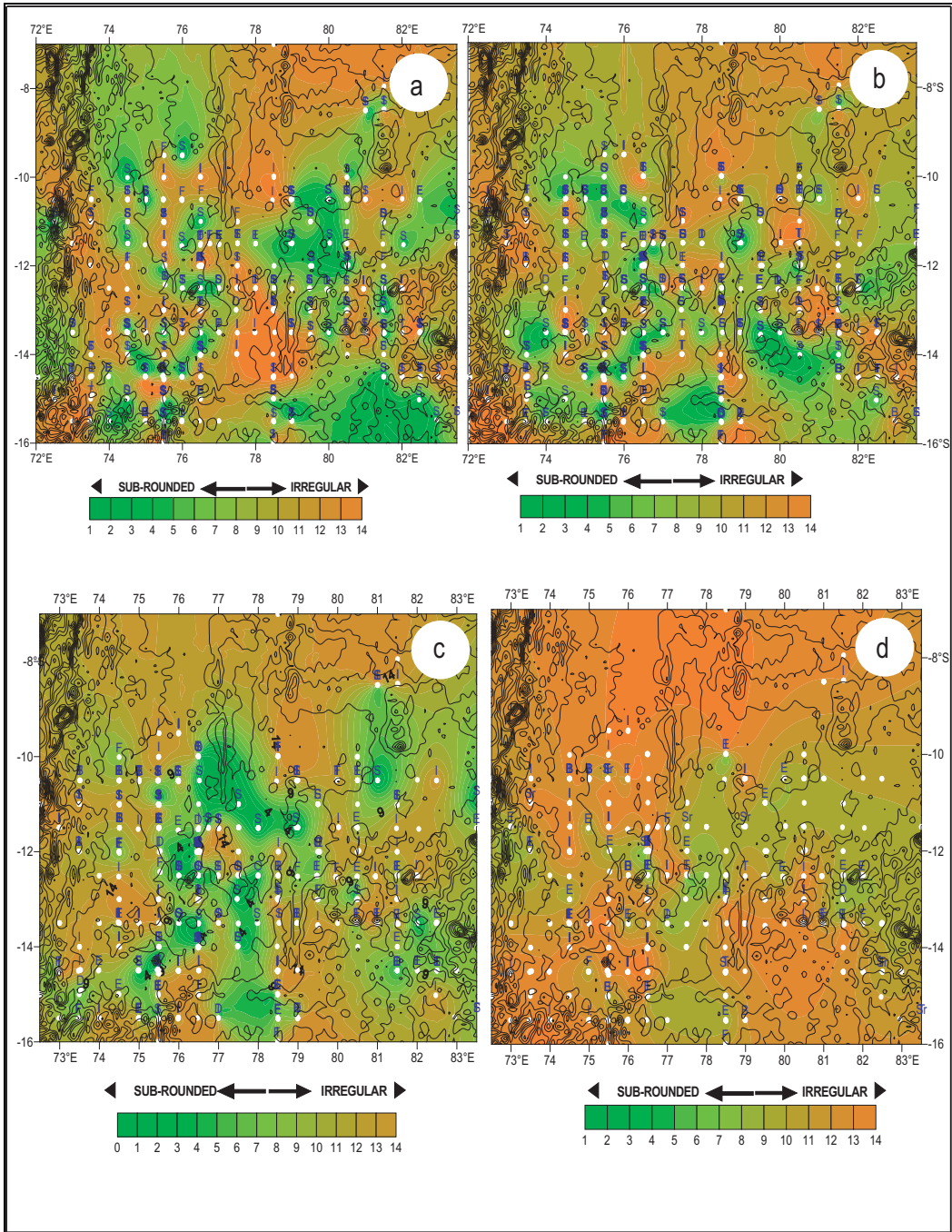
Vineesh et al Figure 3



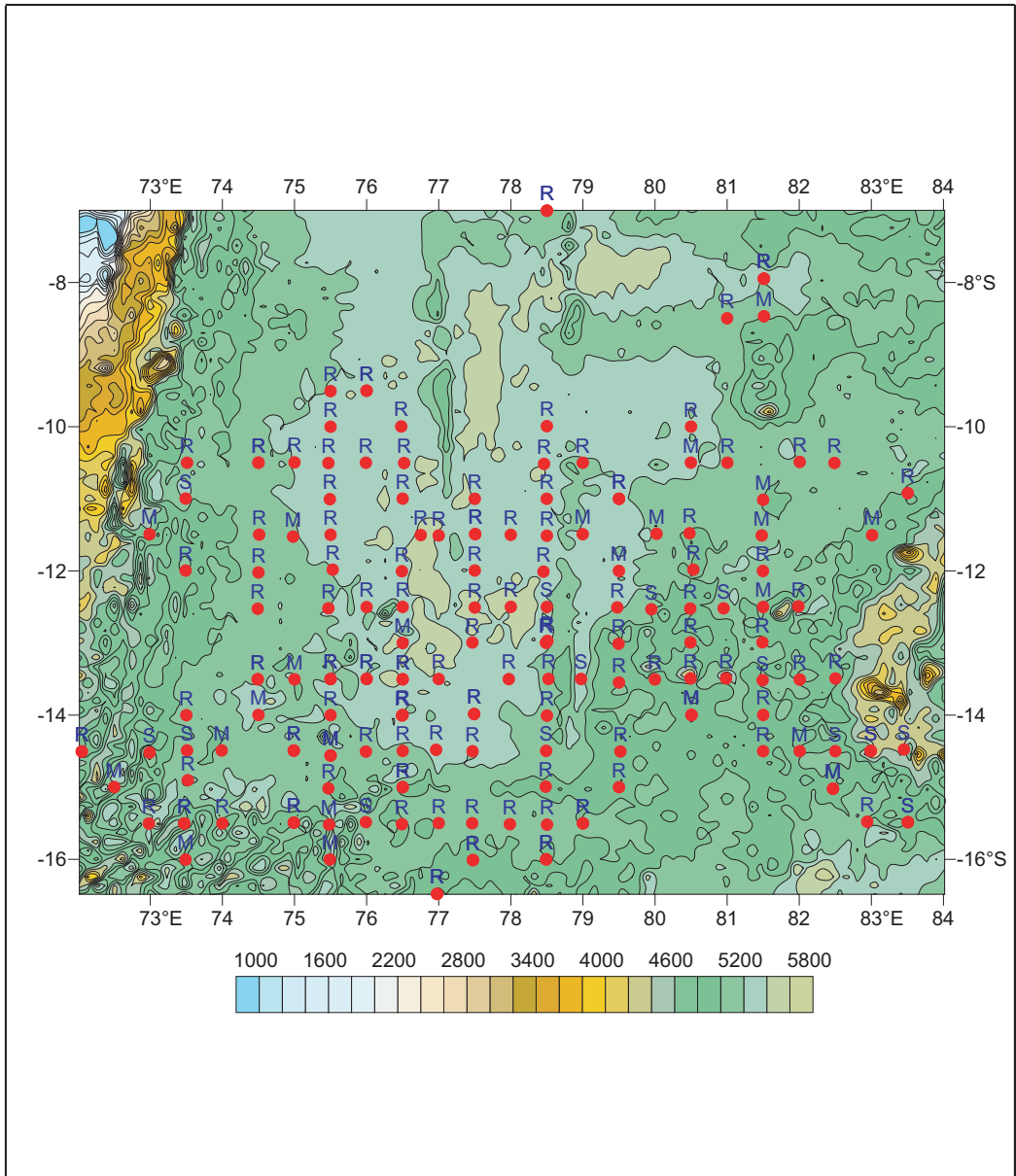
Vineesh et al Figure 4



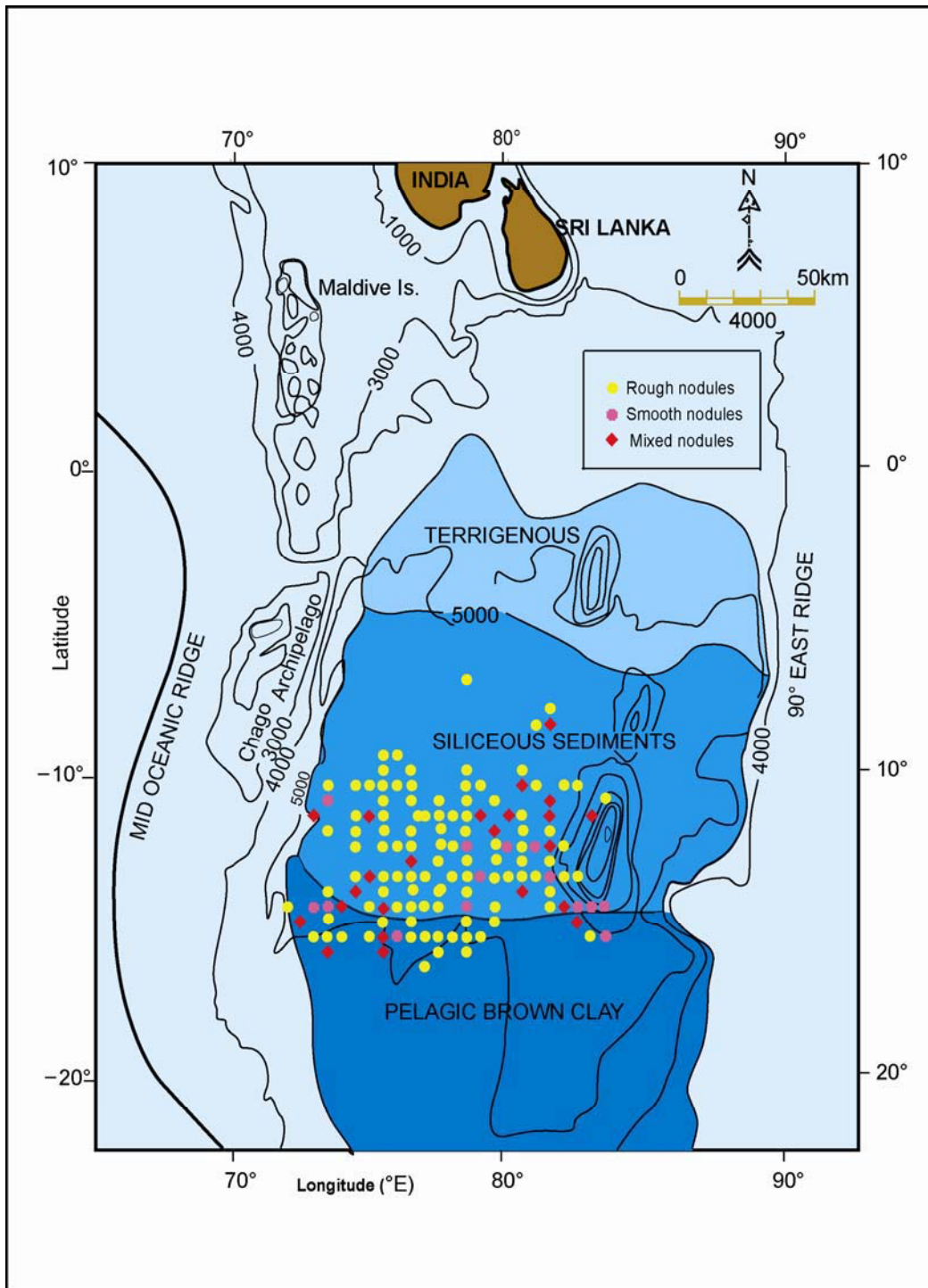
Vineesh et al Figure 5



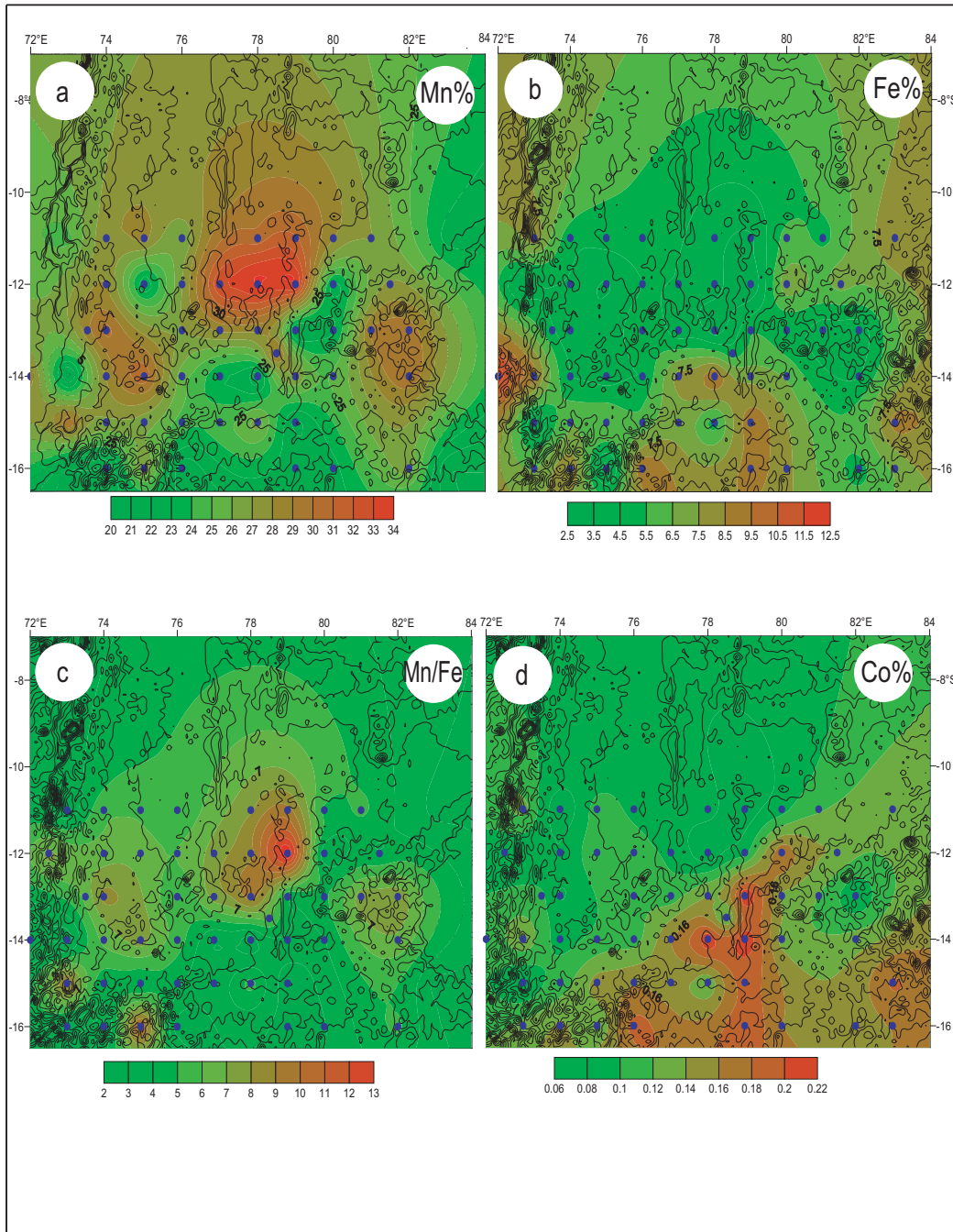
Vineesh et al Figure 6



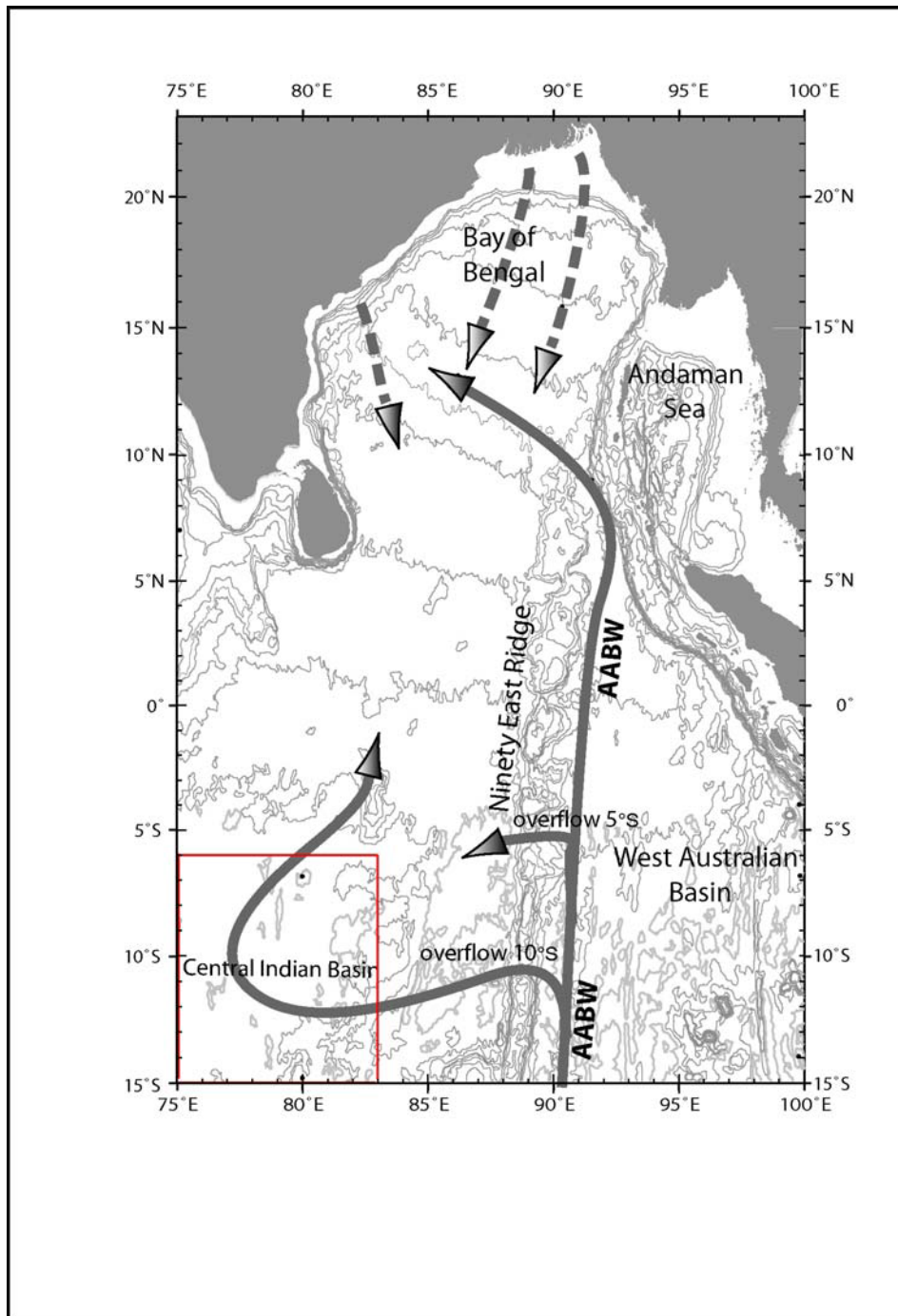
Vineesh et al Figure 7



Vineesh et al Figure 8



Vineesh et al Figure 9



Vineesh et al Figure 10

Table 1. Nodule surface texture related to water depth (m).

a) Smooth surface texture

Sl No.	Latitude	Longitude	Depth (m)	Surface texture
1	-14.476	83.453	4440	S
2	-14.496	82.992	4560	S
3	-14.5	82.5	4800	S
4	-12.532	79.949	4848	S
5	-12.519	80.951	4860	S
6	-15.485	83.507	4860	S
7	-13.515	81.492	4878	S
8	-14.521	72.986	5000	S
9	-13	75.49	5090	S
10	-15.484	75.991	5150	S
11	-14.49	73.508	5150	S
12	-12.5	78.499	5196	S
13	-14.495	78.489	5212	S
14	-10.997	73.494	5379	S
15	-13.499	78.974	5388	S

b) Rough surface texture

Sl No.	Latitude	Longitude	Depth (m)	Surface texture
1	-14.504	72.049	3985	R
2	-10.499	74.501	4581	R
3	-15.503	72.983	4650	R
4	-13.492	82.502	4650	R
5	-14.001	73.499	4691	R
6	-16.479	76.975	4746	R
7	-12.523	80.488	4764	R
8	-13.548	79.499	4800	R
9	-15.491	74.991	4800	R
10	-15.501	79	4800	R
11	-13.492	80.492	4800	R
12	-12.992	80.491	4800	R
13	-10.922	83.505	4815	R
14	-11.478	80.478	4830	R
15	-13.998	81.5	4837	R
16	-13.507	82.007	4848	R
17	-14.5	81.499	4848	R
18	-12.491	81.988	4850	R
19	-13.505	79.998	4860	R
20	-15.519	78.502	4880	R
21	-14.903	73.524	4900	R
22	-12.001	81.496	4908	R
23	-16.01	77.474	4937	R
24	-11.995	73.487	4947	R
25	-15.016	75.472	4950	R
26	-15.5	74	4950	R
27	-13.498	78.522	4956	R
28	-14.504	79.52	4958	R
29	-11.982	80.532	4965	R
30	-15.513	76.493	4966	R
31	-12.499	77.995	4977	R
32	-15.499	77.464	4988	R
33	-13.01	79.494	5000	R
34	-15	79.5	5001	R
35	-12.022	74.5	5025	R
36	-15.513	77.987	5030	R
37	-12.525	74.487	5040	R
38	-15.478	82.943	5040	R
39	-10.489	82.006	5050	R
40	-16	78.491	5050	R
41	-14	75.501	5091	R
42	-14.496	76.5	5100	R
43	-14.999	76.496	5100	R
44	-10.503	82.488	5100	R
45	-10.504	76.518	5100	R
46	-15.502	73.474	5100	R
47	-14.992	78.484	5100	R
48	-12.506	79.476	5112	R
49	-10.5	81.003	5120	R
50	-11.49	77.506	5120	R
51	-11.509	77	5130	R
52	-7.004	78.495	5142	R
53	-15.498	76.998	5150	R
54	-11	77.5	5150	R

55	-14.501	77.469	5152	R
56	-12.518	75.471	5166	R
57	-11.983	75.531	5175	R
58	-13.5	75.498	5186	R
59	-12.995	78.489	5196	R
60	-11.512	78.499	5200	R
61	-14.505	75.994	5200	R
62	-7.948	81.508	5210	R
63	-11.5	77.999	5215	R
64	-11.006	75.488	5239	R
65	-10.5	78.998	5240	R
66	-11.499	75.497	5241	R
67	-8.497	81.002	5250	R
68	-13.997	76.499	5250	R
69	-14.006	76.492	5250	R
70	-13.501	77.972	5250	R
71	-10.495	75	5262	R
72	-12.499	76.496	5269	R
73	-10.5	73.509	5271	R
74	-13.503	76.499	5279	R
75	-9.997	76.484	5280	R
76	-9.501	75.996	5287	R
77	-14.481	76.964	5288	R
78	-10.001	75.496	5296	R
79	-9.993	78.498	5300	R
80	-11	79.5	5300	R
81	-9.999	80.499	5300	R
82	-11.497	74.505	5318	R
83	-11	78.498	5325	R
84	-10.998	76.499	5338	R
85	-12.502	75.999	5340	R
86	-10.516	78.461	5345	R
87	-12.97	78.508	5350	R
88	-9.507	75.501	5360	R
89	-10.504	75.472	5365	R
90	-13.502	74.493	5367	R
91	-12.01	78.453	5381	R
92	-13.499	76.998	5385	R
93	-11.994	77.501	5388	R
94	-13.498	75.997	5393	R
95	-12.005	76.491	5400	R
96	-10.5	75.993	5400	R
97	-14.492	74.993	5400	R
98	-13.985	77.491	5400	R
99	-12.991	81.489	5400	R
100	-10.499	78.984	5400	R
101	-12.508	77.496	5412	R
102	-11.503	76.75	5459	R
103	-12.993	77.467	5460	R
104	-13.491	80.985	5700	R